Phonon-mediated vs. Coulombic Back-Action in Quantum Dot circuits: Electronic Supplementary

D. Harbusch,[1] D. Taubert,[1] H. P. Tranitz,[2] W. Wegscheider,[3] and S. Ludwig[1]

[1] *Center for NanoScience and Fakultät für Physik, Ludwig-Maximilians-Universität München, Geschwister-Scholl-Platz 1, D-80539 München, Germany*

[2] *Institut für Experimentelle Physik, Universität Regensburg, D-93040 Regensburg, Germany*

[3] *Laboratory for Solid State Physics, ETH Zürich, CH-8093 Zürich, Switzerland*

CHARACTERIZATION AND WORKING POINT OF QPC-I

In Suppl. Fig. 1a the relative conductance $G\,/\,G_0$ with $G_0 = 2e^2\,/\,h$ of QPC-I (black solid line, right axis) and its

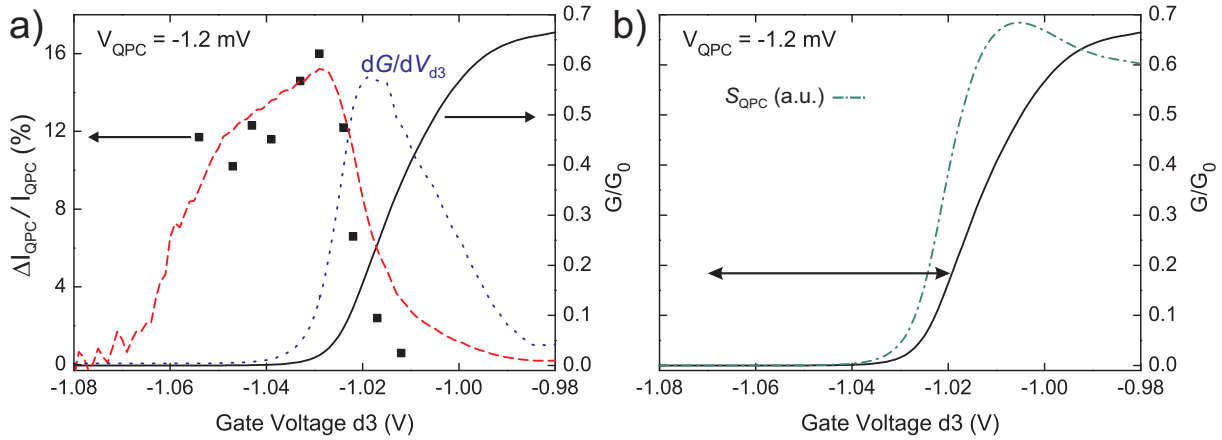

SUPPL. FIG. 1: The black line in a and b plots the conductance (axis on the right) of QPC-I as a function of gate voltage $V_{\rm d3}$. The QPC features a pronounced 0.7 structure, the first plateau is not shown. (a) The blue dotted line is the derivative of the conductance $dG/dV_{\rm d3}$ (in arbitrary units). The red dashed line shows the expected contrast proportional to $\frac{dG/dV_{\rm d3}}{G}$ of the QPC detector calculated from the pinch-off curve (black line). The black squares are direct measurements of the contrast $\Delta I_{\rm QPC}/I_{\rm QPC}$ obtained across the charging lines of QD C, where the charge changes by one electron. (b) The green dashed-dotted line is the expected shot noise spectral density of the QPC in arbitrary units. It is calculated from the pinch-off curve.

derivative $dG\,/\,dV_{\rm d3}$ (blue dotted line) are displayed as a function of gate voltage $V_{\rm d3}$. At maximum derivative the sensitivity of the QPC used as charge detector is highest. The black squares in Suppl. Fig. 1a are the relative changes in the detector current $\Delta I_{\rm QPC}\,/\,I_{\rm QPC}$ measured across a charging line of QD C. It is the contrast of the detector signal. The red dashed line is calculated from the pinch-off curve (black line) with $A_0\frac{dG/dV_{\rm d3}}{G}$, where the overall amplitude A_0 is a free parameter. It marks the detector contrast expected from the pinch-off curve and shows a good agreement with the directly measured data (black squares). Obviously, the contrast of the detector signal is still high at already quite small conductance and small absolute detector sensitivity (blue dotted line). Suppl. Fig. 1b plots the spectral density $S_{\rm QPC} = 2eI_{\rm QPC}(1-\frac{G}{G_0})$ expected for the shot noise of the same QPC (green dashed-dotted line). Clearly, strong shot noise is expected at the point of highest detector sensitivity. Direct back-action related to shot noise has been studied elsewhere [S1,S2] but is not the main focus of this Letter. Instead we focus on a very different indirect back-action mechanism that often outweighs the direct back-action. Accordingly, we disclaim sensitivity and choose a working point of our detector QPC close to pinch-off, where shot noise is weak but the detector contrast is still high. The full range of working points used in the associated Letter is marked by a double arrow in Suppl. Fig. 1b.

In real-time measurements [S3,S4], which need a large detector band-width, it is beneficial to use a detector working point corresponding to a high sensitivity. However, here we show that a substantial investigation of back-action is possible in low bandwidth measurements, where the detector can be used at a smaller sensitivity but less shot noise in the detector circuit.

INFLUENCE OF SYMMETRY PROPERTIES OF THE DOUBLE QD ON THE OBSERVATION OF BACK-ACTION

Suppl. Fig. 2 plots the transconductance $dI_{\rm QPC}/dV_\beta$ in almost identical sections of stability diagrams for two

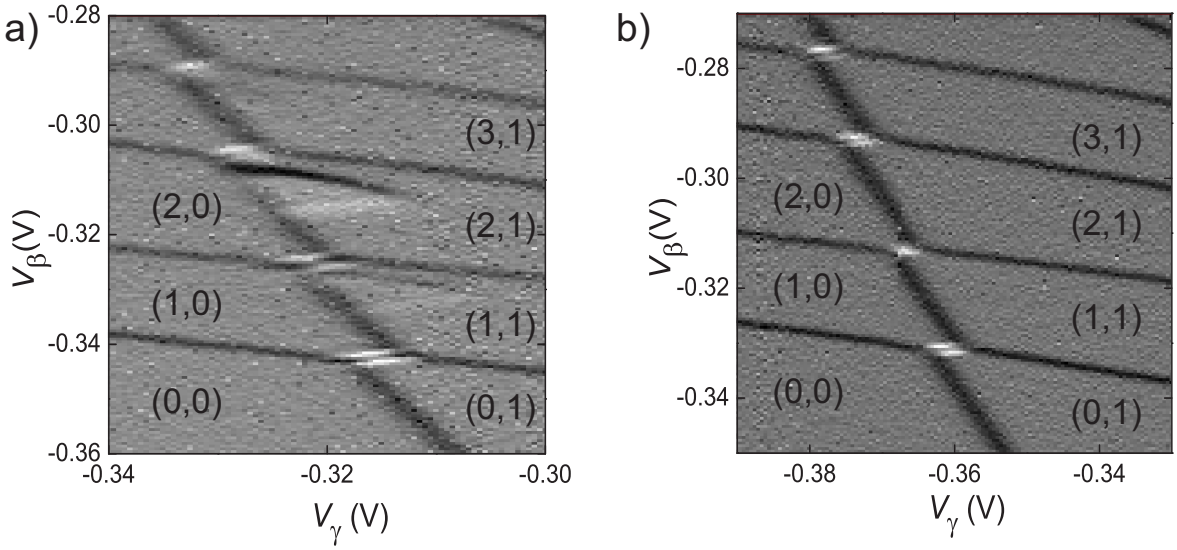

SUPPL. FIG. 2: Transconductance $dI_{\rm QPC}/dV_\beta$ (gray scale) as a function of V_β and V_γ (compare Fig. 1a for the geometry). QPC-I is operated at $V_{\rm QPC} = -0.8\,$mV and $P_{\rm QPC} = 12\,$pW in both measurements. (a) The tunnel couplings between the two QDs and their leads are very different ($V_{\rm t1} = -245\,$mV, $V_{\rm b2} = -350\,$mV); the right tunnel barrier b2 connecting QD C with lead III is almost closed. (b) Analog measurement for more symmetric coupling to the leads ($V_{\rm t1} = -265\,$mV, $V_{\rm b2} = -330\,$mV).

different settings of the voltages applied to gates t1 and b2, which strongly effect the tunnel barriers between the two QDs and their respective leads (compare Fig. 1a of the associated Letter). The bias voltage $V_{\rm QPC}$ applied across QPC-I as well as the dissipated power $P_{\rm QPC}$ are identical for both diagrams. In Suppl. Fig. 2a the barrier b2 between QD C and lead III is almost closed, resulting in a tunneling rate in the kHz-range, whereas the tunneling rate between QD B and lead II as well as the interdot tunneling rate between the two QDs are about five orders of magnitude larger. In contrast, for Suppl. Fig. 2b the tunnel couplings between the two QDs and their respective leads are quite similar. In the asymmetric case shown in Suppl. Fig. 2a we observe two effects caused by absorption of energy, namely the split charge reconfiguration lines (white double lines with positive slopes) and the back-action induced triangles at charge configurations (1,1), (2,1), and weakly at (3,1). In the symmetric case plotted in Suppl. Fig. 2b the back-action induced triangles are missing, while some of the charge reconfiguration lines are still split.

In the following we explain why the back-action induced triangles cannot be observed for symmetric tunnel couplings between the two QDs and their leads (Suppl. Fig. 2). In thermal equilibrium the occupation difference between charge configurations is given by the Boltzman distribution. At the low temperatures in our experiments a Boltzman distribution corresponds to the ground state occupation (everywhere but right at the charging and charge reconfiguration lines). Out of equilibrium deviations from a Boltzman distribution are possible. However, occupation inversion – as observed within the triangles – is only possible if at least three energy states are involved. For the triangles observed in Suppl. Fig. 2a, the three states correspond to the configurations (1,1), (2,0) and (1,0), where (1,1) is the ground state. In case of asymmetric coupling direct transitions (1,0) $\rightarrow$ (1,1) are very slow since the tunnel barrier between QD C and its lead is almost closed (compare sketch in Fig. 1c). The predominant relaxation channel (1,1) $\leftrightarrow$ (2,0) $\leftrightarrow$ (1,0) involves three states, a necessary condition for occupation inversion. And we actually observe back-action induced triangles in Suppl. Fig. 2a. In contrast, for equal tunnel couplings between the QDs and their respective leads the transitions (1,1) $\leftrightarrow$ (1,0) are also possible without additional occupation of an intermediate state (2,0). In particular the reoccupation of the ground state (1,0) $\rightarrow$ (1,1) can happen via one resonant tunneling process of an electron from lead III to QD C. This is the fastest tunneling process involved because it is the only one that doesn't require absorption of energy. As a direct consequence, most of the time the ground state configuration (1,1) is occupied and no back-action induced triangles can be observed (Suppl. Fig. 2b).

The split charge reconfiguration lines measured in transconductance correspond to a double step of the current I_{QPC} along Δ. Between the two parallel lines the current is almost constant at a value suggesting approximately equal population of the two degenerate charge states (e. g. (0,1) and (1,0)). Here, a non-equilibrium energy source (e.g. the QPC) drives rapid oscillations between the two eigen-states, which result from the tunnel coupling between the two localized states (0,1) and (1,0). The rapid oscillations cease, if the energy splitting $E = \sqrt{\Delta_0^2 + \Delta^2}$ between the eigen-states exceeds the maximum available energy E_{max}, where Δ_0 is the interdot tunnel splitting and Δ the asymmetry energy between the localized states (0,1) and (1,0). In addition, the energy relaxation rate decreases with increasing $|\Delta|$ because as the eigen-states converge into the localized states (0,1) and (1,0), the overlap of the wavefunctions reduces. The distance between the split charge reconfiguration lines is determined by these two conditions. Here, we omit discussing the ratio of the interdot tunneling rate with the respective tunneling rates between the two QDs and their leads. However, in the experiments discussed here, the interdot tunnel coupling exceeds the couplings between the QDs and their leads.

Note that the charge reconfiguration line between the states (2,0) and (1,1) in Suppl. Fig. 2b is not split. Here, Pauli spin-blockade is possible [S5]. Under certain conditions spin-blockade can strongly reduce interdot tunneling. As a consequence, the otherwise observed rapid oscillations are absent and the reconfiguration line is not split. We have not observed any spin-blockade related effects on the back-action induced triangles.

STRONGLY DRIVEN QPC-I (PHONON-MEDIATED VS. COULOMBIC INTERACTION)

Fig. 3a of the associated Letter shows only one back-action induced triangle, while Fig. 3b contains two triangles. As described in the Letter, the upper triangle can be allocated to energy absorption in QD C while the lower triangle is related to energy absorption in QD B. From these measurements one could conclude that phonons emitted in the leads of QPC-I can only excite QD C (resulting in the upper triangle) while phonons emitted from QPC-II are absorbed by both QDs (resulting in two triangles). However, in the first case (Fig. 3a) QPC-I is weakly biased with $P_{\mathrm{QPC}} = 2.5\,\mathrm{pW}$, while for Fig. 3b QPC-II is driven much stronger, namely at $P_{\mathrm{QPC}} = 72\,\mathrm{pW}$. Suppl. Fig. 3a plots a

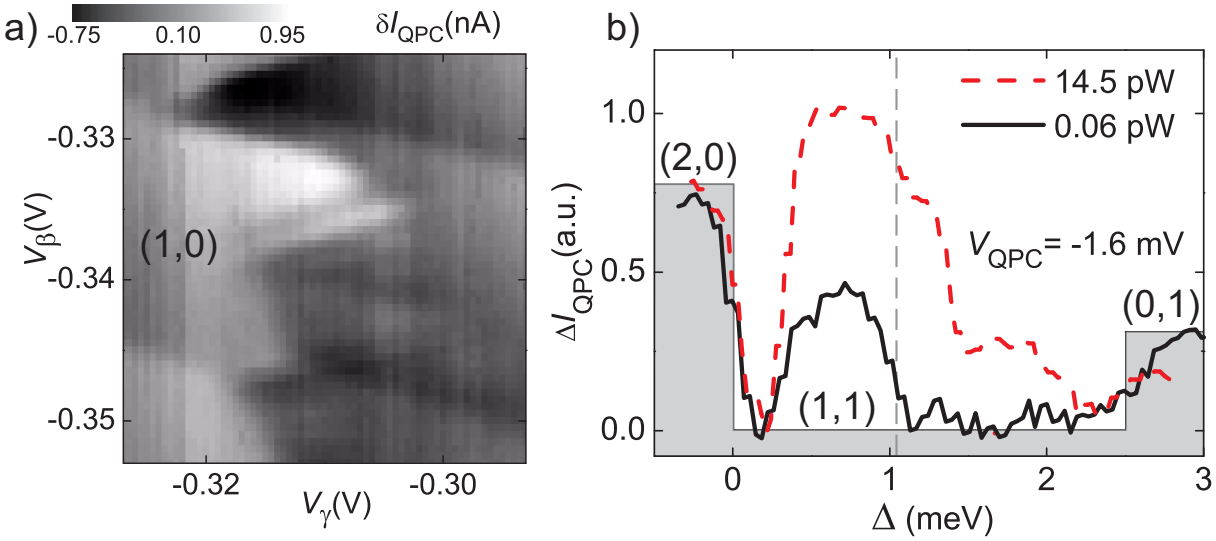

SUPPL. FIG. 3: (a) δI_{QPC} (gray scale) as a function of V_β and V_γ. A plane fit is subtracted from I_{QPC}. Here QPC-I is the emitter operated at $V_{\mathrm{QPC}} = -1.6$ mV and $P_{\mathrm{QPC}} = 14.5\,\mathrm{pW}$. (b) Normalized current change ΔI_{QPC} versus asymmetry energy Δ for QPC-I at $V_{\mathrm{QPC}} = -1.6\,\mathrm{mV}$. More details in Fig. 3 of the associated Letter.

comparable section of the stability diagram with QPC-I being strongly driven ($V_{\mathrm{QPC}} = -1.6\,\mathrm{mV}$, $P_{\mathrm{QPC}} = 14.5\,\mathrm{pW}$). In this case the upper triangle is clearly visible, but in addition the second (lower) triangle starts to appear. In Suppl. Fig. 3b two measurements comparable to those in Fig. 3d of the associated Letter are shown. The power dissipated in QPC-I is $P_{\mathrm{QPC}} = 0.06\,\mathrm{pW}$ for the solid line and $P_{\mathrm{QPC}} = 14.5\,\mathrm{pW}$ for the red dashed line (taken from the measurement shown in Suppl. Fig. 3a), while $V_{\mathrm{QPC}} = -1.6\,\mathrm{mV}$ in both cases. The smaller maximum at an asymmetry energy of $\Delta \sim 1.8\,\mathrm{meV}$ belongs to the lower triangle. Nevertheless, this phonon induced maximum is superimposed by the high energy contributions of the upper triangle (also seen in Suppl. Fig. 3a), which are caused by indirect Coulomb

interaction and are related to the excitation spectrum of QD C, as discussed in the associated Letter.

In conclusion, phonons can be reabsorbed in both QDs no matter where they have been emitted. However, the magnitude of phonon-mediated back-action strongly depends on the detailed geometry. In our experiments the relevant phonons are emitted by relaxation of excited charge carriers in the leads of the driven QPC. For the energies typical for our measurements, the excited charge carriers usually scatter with the cold Fermi-sea before an acoustic phonon can be emitted. Energies and directions of the emitted phonons, in turn, depend on the energies and momenta of the excited charge carriers. In addition the anisotropic coupling tensors for electron-phonon interaction play a critical role [S6,S7]. In particular, phonons are emitted much stronger along certain crystal directions than other directions. While a quantitative analysis goes beyond the scope of this paper, these considerations explain, why the absorption strength of phonons in specific locations (QDs) strongly depends on the detailed geometry of emitter and detector.

For $\Delta \lesssim 1.04\,\mathrm{meV}$, where we identified phonon-mediated interaction as the main coupling mechanism, features related to the excitation spectrum of QD C are missing (e. g. Fig. 2a), even so excited states are expected to exist for $\Delta \lesssim 1.04\,\mathrm{meV}$. We can speculate that the absorption of phonons is accompanied with a level broadening that in turn prevents us from resolving the excitation spectrum. However, the microscopic details of this observation are not yet understood. Nevertheless, the phenomenological difference between the two discussed regimes ($\Delta \lesssim 1.04\,\mathrm{meV}$ and $\Delta > 1.04\,\mathrm{meV}$) can be taken as a hint, that in our experiments back-action caused by two different coupling mechanisms is observed.

With QPC-II as emitter (Figs. 3b and 3e) we find only one of the two back-action mechanisms, namely the phonon-mediated back-action observed for $\Delta \lesssim 1.04\,\mathrm{meV}$. In fact, the second mechanism still seen for $\Delta > 1.04\,\mathrm{meV}$ has only been observed with QPC-I as emitter and the energy being absorbed in QD C. An important difference between the two QPCs is their capacitive coupling to the QDs. The strongest capacitive coupling exists between QPC-I and QD C. In detail, a difference of one electron in QD C causes a shift of the local potential at QPC-I by approximately $5\,\mu\mathrm{eV}$. The capacitive coupling between one of the leads of QPC-I (lead III) and QD C is expected to be even stronger. The fact that we observe the excitation spectrum of QD C only when QPC-I is strongly biased (Figs. 2a and 3c) indicates, that for $\Delta > 1.04\,\mathrm{meV}$ Coulomb interaction is probably the predominant coupling mechanism involved. However, $E_{\max} < eV_{\mathrm{QPC}}$ (closed circles in Fig. 2c) is in contradiction to the expectation for direct Coulomb interaction between the QPC and the double QD. An indirect Coulomb interaction is possible via excited charge carriers, while they are reflected at the tunnel barrier between QD C and lead III (compare Fig. 1a in the associated Letter). The energy stems from "hot" electrons injected from QPC-I into lead III and relaxed via scattering with the Fermi-sea in lead III. The relaxation processes shift the energy spectrum compared to that directly emitted by the QPC.

[S1] Onac *et al.,* Phys. Rev. Lett. **96**, 176601(2006)
[S2] Gustavsson *et al.,* Phys. Rev. B **78**, 035324(2008)
[S3] Gustavsson *et al.,* Phys. Rev. Lett. **96**, 076605 (2006)
[S4] Flindt *et al.,* PNAS **106**, 10116(2009)
[S5] Ono *et al.,* Science **297**, 1313 (2002)
[S6] H. Karl *et al.,* Phys. Rev. Lett. **61**, 2360(1988)
[S7] D. Lehmann *et al.,* Phys. Rev. B **65**, 085320 (2002)